J Nanostruct 16(2): 2288-2300, Spring 2026

RESEARCH PAPER

Structural and Optical Modulation of ZnS-ZnO/PVA Nanocomposite Films with Enhanced UV-Shielding

*Header Thajeel Khammat, Mahasin F. Hadi Al-Kadhemy *, Khaldoon N. Abbas*

Physics Department, College of Science, Mustansiriyah University, Baghdad, Republic of Iraq

ARTICLE INFO

Article History:
Received 10 December 2025
Accepted 26 March 2026
Published 01 April 2026

Keywords:
Hydrothermal synthesis
Optical bandgap tuning
ZnS-ZnO/PVA nanocomposite films
ZnS-ZnO nanoparticles
UV-Vis spectra

ABSTRACT

This study successfully achieved the synthesis of binary ZnS-ZnO nanocomposite using a controlled hydrothermal method. Following nanocomposite synthesis, pure PVA film and ZnS-ZnO/PVA films were fabricated by incorporating the ZnS-ZnO nanocomposite into the PVA matrix at different doping levels of (0.6 and 1 wt%) via the solution casting technique. Consequently, three samples were successfully produced using the casting method, exhibiting good homogeneity, free-standing nature, and satisfactory mechanical stability. Structural characterization by X-ray diffraction (XRD) confirmed the semicrystalline nature of the pure PVA matrix with the successful nanoscale incorporation of ZnS-ZnO NPs. Morphological analysis using the FESEM technique revealed a relatively uniform dispersion of nanoparticles at the lower loading level (0.6 wt%), while partial agglomeration was observed at the higher loading (1 wt%) of ZnS-ZnO Nps. Additionally, UV-Vis spectra inspection of as-prepared ZnS-ZnO/PVA films demonstrated that the incorporation of ZnS-ZnO NPs led to a significant enhancement in ultraviolet absorption while maintaining high transparency in the visible region. The effective optical bandgap values were estimated from Tauc plots, showed a gradual decrease from 4.48 eV to 4.36 eV with increasing ZnS-ZnO NPs content. This reduction is attributed to the formation of interfacial states, defect-related energy levels, and enhanced electronic coupling between the ZnS-ZnO NPs and the PVA polymer matrix.

How to cite this article
Thajeel Khammat H., Hadi Al-Kadhemy M., Abbas K. Structural and Optical Modulation of ZnS-ZnO/PVA Nanocomposite Films with Enhanced UV-Shielding . J Nanostruct, 2026; 16(2):2288-2300. DOI: 10.22052/JNS.2026.02.073

INTRODUCTION

Among nanoscale semiconductor materials, zinc sulfide (ZnS) and zinc oxide (ZnO) are two prominent wide-bandgap semiconductors that have attracted substantial scientific and technological interest due to their outstanding structural, optical, and electronic properties. ZnS is characterized by a wide direct band gap of approximately 3.6 eV and a high exciton binding energy, which makes it highly suitable for optoelectronic devices, photocatalysis, and sensing applications. On the other hand, ZnO exhibits a wide band gap of about 3.37 eV at room temperature, along with excellent catalytic activity, chemical stability, and favorable electrical and photochemical properties, enabling its extensive use in diverse technological fields. The integration of ZnS and ZnO nanostructures into a nanocomposite system has emerged as an effective strategy to synergistically combine their individual advantages while overcoming their inherent limitations [1-3].

* *Corresponding Author Email: dr.mahasin@uomustansiriyah.edu.iq*

The formation of ZnS-ZnO heterostructures can promote efficient charge separation at the interface, suppress electron-hole (*e*-*h*) recombination, and enhance light absorption and carrier transport, leading to improved functional performance compared to the individual components. These synergistic effects render ZnS-ZnO nanocomposites highly promising for advanced applications such as photocatalysis, optoelectronic, environmental, and sensing applications. Furthermore, the tuneable band alignment and interfacial interactions between ZnS and ZnO structures provide a versatile platform for modifying the physical properties of the composite at the nanoscale. Consequently, controlled synthesis of ZnS-ZnO nanocomposites with specific physical properties has become a pivotal point of current investigation, particularly using solution-based methods that enable precise control over morphology, phase composition, and interfacial characteristics. A variety of synthetic approaches have been developed to produce ZnS-ZnO nanostructures such as nanoparticles, nanowires, nanorods etc., including CVD methods [4-6], sol-gel route [1], electrochemical deposition [7, 8], as well as solvothermal and hydrothermal routes [9, 10], etc. Among these approaches, the hydrothermal method is regarded as one of the most favorable techniques due to its simplicity, cost-effectiveness, high yield, and its ability to achieve well-defined and controllable nanostructures [9, 11-13].

Furthermore, polyvinyl Alcohol (PVA) is a widely used synthetic polymer in scientific and industrial applications due to its favourable physicochemical properties and environmental compatibility [14] Chemically, PVA consists of repeating units $[–CH_2–CH(OH)–]_n$, where the presence of hydroxyl (^-OH) groups plays a critical role in governing its physical and chemical behaviour. These hydroxyl groups facilitate strong intermolecular hydrogen bonding, resulting in high water solubility, excellent adhesive properties, and enhanced compatibility with inorganic nanomaterials. PVA is typically produced via the hydrolysis of polyvinyl acetate, with its final properties strongly influenced by both the degree of hydrolysis and molecular weight[15]. The physical and optical characteristics of PVA make it particularly attractive for polymeric matrices in nanocomposite systems. It is colorless, non-toxic, biocompatible, and biodegradable, exhibiting high optical transparency in the visible range. Additionally, PVA demonstrates good thermal stability and chemical resistance, enabling its use in optical films, membranes, sensors, and biomedical devices. Its excellent film-forming ability also allows the fabrication of uniform, flexible thin films with controlled thickness [16]. In ZnS-ZnO nanocomposite systems, PVA functions not only as a supportive matrix but also as a stabilizing agent that prevents nanoparticle agglomeration and promotes uniform dispersion. Strong interactions between the ZnS-ZnO nanostructures and the hydroxyl groups of PVA enhance photostability, mechanical integrity, and the optical performance of the nanocomposite

The present study aims to develop ZnS-ZnO/PVA nanocomposite films and to systematically investigate the influence of ZnS-ZnO nanoparticle with different ratios (0.6 to 1% wt) incorporation on the structural, morphological, and optical properties of the PVA matrix. The motivation for this work stems from the shortage of systematic studies addressing interfacial interactions and band-gap modulation in PVA-based ZnS-ZnO heterostructured polymer nanocomposites. Despite the growing interest in semiconductor-polymer hybrid systems, the combined influence of nanoparticle dispersion, crystallinity, and heterojunction formation on the optical response of ZnS-ZnO/PVA matrices remains insufficiently explored. By establishing a clear correlation between structural characteristics and optical behavior, this study offers new insights into the controlled design of UV-responsive polymer nanocomposites while maintaining high visible transparency. The outcomes of this work are anticipated to support the development of flexible optoelectronic and UV-shielding materials with improved performance, durability, and functional stability.

MATERIALS AND METHODS

Materials

All chemicals employed in this study were of analytical grade and were used without any further purification. Zinc nitrate hexahydrate ($Zn(NO_3)_2·6H_2O$, Hi Media Laboratories Pvt. Ltd., India), sodium hydroxide (NaOH, SD Fine-Chem Limited (SDFCL), Mumbai, India), Sodium Sulfide (Na_2S), Hi-media India, and Hexamethylenetetramine (HMT, Loba Chemie, India) were utilized as received. Moreover, Polyvinyl alcohol (PVA) polymer, Central House Company, India) and analytical-

grade absolute ethanol (Scharlau, Scharlab S.L., Barcelona, Spain) as well as distilled water (DW) were also used without further treatment.

Synthesis of ZnS-ZnO Nanoparticles

ZnS-ZnO nanoparticles (NPs) were prepared using a simple hydrothermal method, under short reaction time conditions (1 h) and a pH value of their precursor solutions (12), with the possibility of adding HMT at a rate of 20% of the total solution to study its effects on the physical and chemical properties of as-prepared samples. Initially, equimolar aqueous solutions (1.5 M) of zinc nitrate hexahydrate ($Zn(NO_3)_2{\cdot}6H_2O$) and sodium sulfide (Na_2S) were prepared in 80 mL of distilled water. These solutions were then combined and stirred magnetically at room temperature (RT) for 30 minutes to ensure complete homogenization of the metal ions. Later, hexamethylenetetramine (HMT) was added at a concentration of 0.1 M and in an amount equal to 20% of the total volume of the base reactant solution, and stirring was continued for an additional 30 minutes to facilitate the formation of a homogeneous compound. The pH of the base solution was adjusted to 12 by the gradual addition of 0.1 M sodium hydroxide (NaOH) with continuous stirring. The resulting suspensions were then transferred to autoclaves and subjected to hydrothermal treatment at 100 °C for 1 hour. After being left to naturally cool to room temperature, the precipitates were successively washed with ethanol and distilled water to remove unreacted species and residual by-products. After each washing step, centrifugation was performed at 4000 rpm for 30 minutes to ensure effective separation of the solid phase. The washed samples were dried in an oven at 80 °C for 6 hours, followed by calcination at 500 °C for 3 hours in an air-covered furnace. (Fig. 1).

Synthesis of ZnS-ZnO/PVA Nanocomposites Films

ZnS-ZnO/PVA nanocomposites films were prepared using the solution casting technique. Initially, a PVA solution was prepared by dissolving 0.5 g of PVA in 15 mL of distilled water under continuous magnetic stirring at RT until a homogeneous solution was obtained. Subsequently, ZnS-ZnO NPs were incorporated into the PVA solution at different weight ratios (0.6 wt% and 1 wt%) and stirred continuously for 1 h to ensure preliminary mixing. To improve ZnS-ZnO nanoparticle (NPs) dispersion and minimize agglomeration within the polymeric matrix, the resulting suspensions were subjected to ultrasonic treatment for 30 min, followed by further magnetic stirring for 2 h to achieve uniform distribution of ZnS-ZnO NPs throughout the PVA solution. The homogeneous mixtures were then poured into clean glass containers and allowed to dry at room temperature for 7 days. After complete

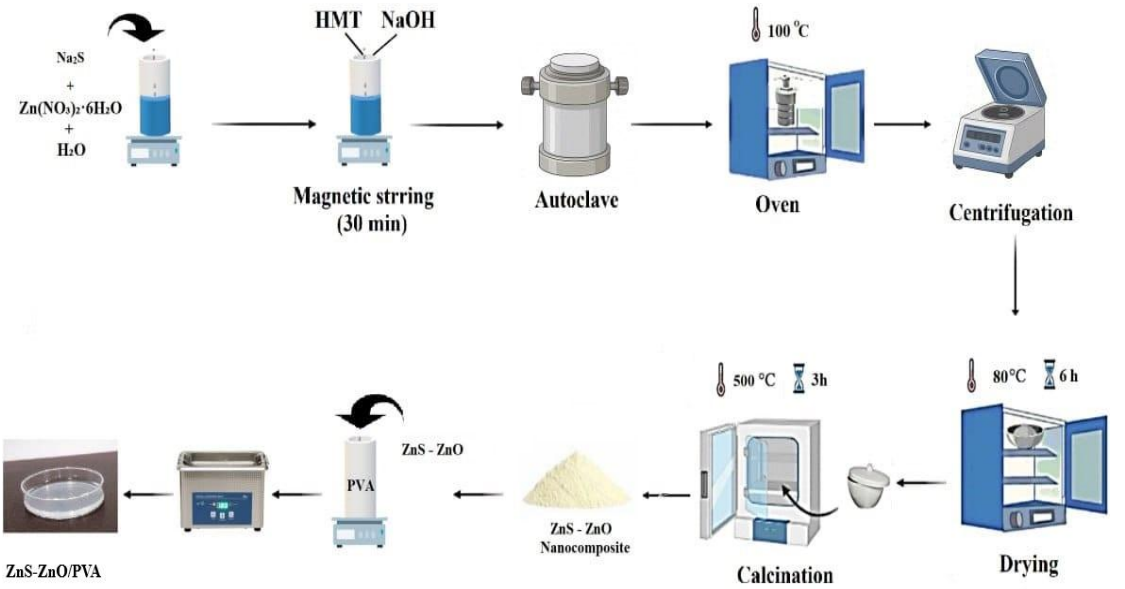

Fig. 1. Schematic illustration of the preparation procedure for ZnS-ZnO and ZnS-ZnO/PVA nanocomposite films.

solvent evaporation, the flexible ZnS-ZnO/PVA nanocomposite films with different nanoparticles loadings (0.6 wt% denoted as sample P1) and (1 wt% denoted as sample P2) were carefully peeled off and stored in sealed containers for subsequent characterization (Fig. 1).

Characterization

The structural, morphological, and optical properties were investigated for ZnS-ZnO/PVA films samples, X-ray diffraction (PXRD) was employed to examine the crystalline structure using an X'Pert diffractometer (Malvern Analytical, Netherlands) equipped with a Cu-Kα radiation source (λ = 1.5418 Å). The diffraction data were collected over a 2θ range of 10°–80°, with a scanning rate of 10°/min and a step size of 0.04°, providing adequate resolution for reliable phase identification and crystallite size estimation. Surface morphology was analyzed using a field-emission scanning electron microscope (FESEM, Tescan MIRA3). Finally, the optical absorption spectra were recorded with a UV-Vis spectrophotometer (PG Instruments Limited, model T70/T80) in the wavelength range of (200-800) nm. The obtained UV-Vis results were subsequently used to estimate the optical energy band gap (Eg) using the Tauc plot for the as-prepared samples.

RESULTS AND DISCUSSIONS

XRD Analysis

X-ray diffraction patterns (Fig. 2) were used to identify the crystalline phase and structural development of ZnS-ZnO binary nanocomposite sample prepared under synthesis conditions (pH 12 and 1 h growth time). The XRD results reveal the presence of several coexisting crystalline phases, including cubic ZnS (zinc blende), hexagonal ZnS (wurtzite), and hexagonal ZnO, indicating that phase formation is significantly influenced by the growth environment and post-synthesis treatment.

Importantly, XRD pattern in the Fig.2 shows a strong dominant peak at 28.43°, which corresponds to the (002) plane of hexagonal ZnS (wurtzite), indicating a preferential orientation of this phase. The additional peaks at 47.44° and 56.19° are attributed to the (220) and (331) planes of cubic ZnS (zinc blende). The observed reflections at 31.41°, 34.04°, 35.89°, 62.37°, and

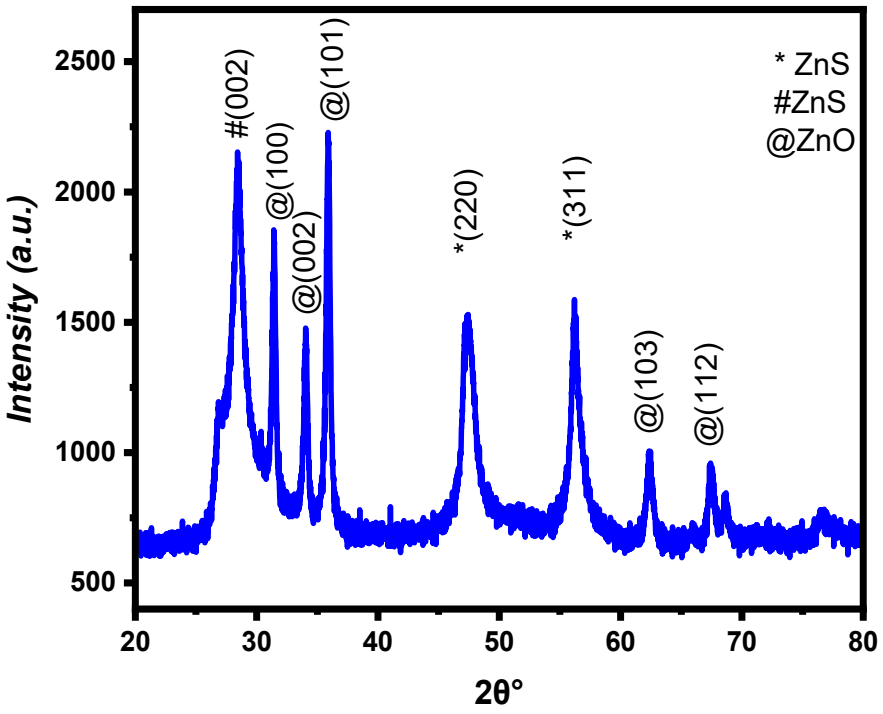

Fig. 2. X-ray diffraction (XRD) patterns of the ZnS-ZnO binary nanocomposite (pH 12, growth time 1 h, and 20% HMT).

67.32° correspond to the (100), (002), (101), (103), and (112) planes of hexagonal ZnO [17-19].

X-ray diffraction (XRD) analysis reveals the formation of a well-defined crystalline nanostructure with a high degree of crystallinity. The sharp and distinct peaks obtained indicate the polycrystalline nature of the sample and confirm the successful formation of stable nanocrystals during the brief preparation period (1 h). A direct relationship can be established between the changes in crystallite size (D nm) and dislocation density (δ), as listed in Table 1, and the hydrothermal synthesis parameters, particularly solution pH, growth time, and HMT content, compared to the results of previous studies [20-22]. These parameters influence the balance between nucleation, growth, and crystal aggregation during the formation of ZNS-ZnO. Additionally, the crystallite sizes D of all samples were determined based on the dominant crystalline peak, calculated using Scherrer's formula (Eq. 1), as follows [23]:

$$D = \frac{\mathrm{K}\,\lambda}{\beta\cos\theta} \quad (1)$$

Where D (nm) is the crystallite size and K (0.9) is the shape factor. The β represents the full width at half maximum (FWHM) of the diffraction peak, expressed in radians and θ represents the Bragg angle. Also, the number of dislocations (δ) was calculated using the Eq. 2 [24].

$$\delta = \frac{1}{D^2} \quad (2)$$

The obtained results as shown in Table 1 include calculated crystallite sizes reveal that the ZnO phase exhibits larger crystallites (from 15 to 24 nm) compared to the ZnS phase (from 6 to 11 nm). That indicating enhanced crystal growth and structural stability of ZnO within the composite matrix. The relatively lower FWHM values observed for ZnO peaks propose improved crystallinity and reduced lattice imperfections, which is further supported by the lower dislocation density values (Table 1). In contrast, the higher FWHM value and dislocation density associated with ZnS reflections imply smaller crystallite domains and increased defect concentration, which can be attributed to lattice mismatch and interfacial strain between the ZnS and ZnO phases [25, 26].

The current results confirm that high pH promotes rapid nucleation, leading to the formation of small, uniformly distributed nanocrystals. while, The short growth period limited the complete development of the crystals, resulting in nanoscale particles that were still fairly uniform and maintained a stable crystalline structure, HMT played a key role in controlling crystal growth by slowly releasing hydroxide

Table 1. The Crystallite size (D), FWHM, and dislocation density (δ) values of as-grown ZnS-ZnO nanocomposite.

Sample(s)	(*h k l*)	2Θ Exp. (Deg.)	2Θ JCPDS (Deg.)	FWHM (Deg.)	D (nm)	δ x 10^{11} (cm^{-2})
#ZnS	002	28.43	28.50	1.06	7.73	16.72
	100	31.41	31.77	0.41	20.12	2.46
	002	34.04	34.42	0.39	21.30	2.20
@ZnO	101	35.89	36.25	0.35	23.85	1.75
	103	62.37	62.68	0.59	15.73	4.03
	112	67.32	67.96	0.53	18.0	3.08
	220	47.44	47.52	0.81	10.71	8.71
*ZnS	331	56.19	56.29	1.46	6.16	26.28

ions (OH^-), which helped regulate the nucleation process, minimize structural defects, and improve the overall crystallinity of the sample, which is coinsseset with hte litruture results [27]. Overall, the combination of these factors produced ZnS-ZnO nanocomposite as a well-crystallized, polycrystalline nanostructure with consistent particle sizes and high purity.

FESEM Analysis

Fig. 3A-B shows the FESEM micrograph of the as-grown ZnS-ZnO nanoparticles, which reveals the formation of a distinct nanostructured surface with relative homogeneity. The observed surface from FESEM (Fg. 3B) image is predominantly composed of ultrafine, quasi-spherical nanoparticles with closely distributed sizes, forming a dense granular nanostructure across the substrate. These primary nanoparticles appear to be tightly packed, giving rise to a continuous nanoscale network. In addition, intermittently distributed some agglomerates (EFSEM image, Fig. 3A) are evident, which likely originate from the partial coalescence of adjacent nanoparticles during the growth process. Despite their presence, these agglomerates do not disrupt the overall uniformity of the nanostructure, indicating that excessive particle aggregation was effectively suppressed. This morphological behaviour can be attributed to the **s**trongly alkaline environment (pH = 12)**,** which promotes rapid yet stabilized nucleation of zinc-based species. Under such conditions, the high concentration of hydroxyl (OH^-) ions facilitates the simultaneous formation of ZnS and ZnO phases**,** leading to the development of a binary ZnS-ZnO system. The coexistence of these two phases contributes to the observed variation in particle contrast and size, reflecting differences in growth kinetics between the sulfide and oxide components [28].

Furthermore, the incorporation of HMT at 20% plays a critical role in regulating the reaction dynamics. Acting as a slow-release source of (OH^-) ions, HMT moderates the local chemical environment, enabling controlled crystal growth and limiting uncontrolled nucleation events. Consequently, the nanocomposite evolves toward a finely divided morphology with improved structural stability. Also, the short reaction time (1 h) restricts prolonged crystal ripening, preserving the nanoscale dimensions of the particles and preventing the formation of larger, well-faceted micro/nanostructures.

Thus the resulting morphology-characterized by high nanoparticle density, moderate antiparticle porosity, and extensive interfacial contact between ZnS and ZnO phases is highly advantageous. Such structural features are known to enhance surface-dependent processes, particularly by facilitating efficient charge transfer across heterojunction interfaces. Overall, that makes the synthesized ZnS-ZnO nanocomposite a promising candidate

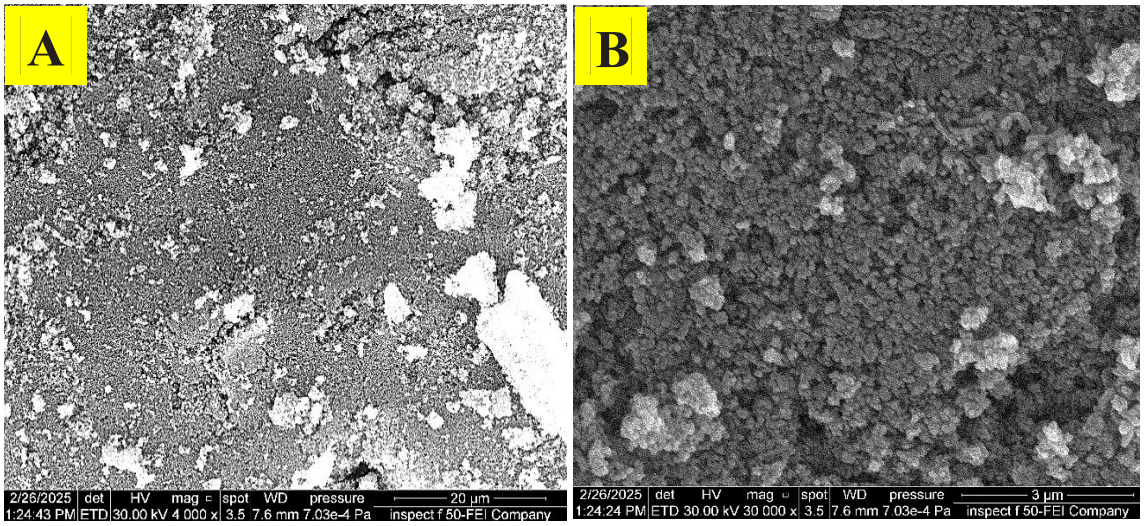

Fig. 3. A-B: FESEM images of ZnS-ZnO nanocomposite synthesized by hydrothermal method at growth time 1h, precursor pH (12) and growth temperature 100 °C.

for applications in photocatalysis, optoelectronic devices, and sensing technologies [29, 30].

Optical Properties

The UV-Vis absorption spectrum presented in Fig. 4 illustrates the optical behavior of the ZnS-ZnO sample across the (200-800 nm) spectral regions. The UV-Vis spectrum exhibits a pronounced absorption peak around 365-370 nm, indicative of the formation of homogeneous nanostructured phases for both ZnS and ZnO, with electronic transitions corresponding to the intrinsic band structures of each constituent. The effective optical band gap (E_g) was estimated from the corresponding Tauc plot through the relationship between $(\alpha h\nu)^2$ and $h\nu$, assuming a direct transition, with E_g approximately 2.94 eV. The extracted direct band gap lies lower those of ZnO (~3.3 eV) and ZnS (~3.6 eV) indicating that the optical absorption of the ZnS-ZnO nanocomposite is governed by the combined contribution of both phases and their interfacial interactions [1]. The observed red-shift relative to pure ZnO can be attributed to interfacial defect states, band bending, and type-II band alignment at the ZnS/ZnO heterointerface rather than the dominance of a single phase.

XRD analysis of ZnS-ZnO/PVA Film

Fig. 5 presents the X-ray diffraction (XRD) patterns of the pure PVA film and for ZnS-ZnO/PVA films with different ZnS-ZnO nanoparticles loadings (P1 6wt% and P2 1wt%). Both nanocomposite samples exhibit a broad and intense diffraction peaks centered at $2\theta \approx 18.54^{\circ}$ for P1 and 19.13° for P2 samples, which is characteristic of the semi-crystalline structure of polyvinyl alcohol (PVA). This feature confirms the dominance of the amorphous PVA matrix, with the presence of small ordered crystalline domains originating from intermolecular hydrogen-bond interactions between PVA chains. From Fig. 5 at lower ZnS-ZnO loading in sample P1 6wt% no distinct XRD peaks corresponding to ZnS or ZnO are observed. This indicates that the ZnS-ZnO nanoparticles are either ultra-fine or highly dispersed within the polymer matrix, lacking long-range crystalline order detectable by XRD. Such behaviour suggests strong confinement of ZnS-ZnO nanocomposite by the PVA matrix, which effectively suppresses crystal growth and aggregation at low filler concentrations.

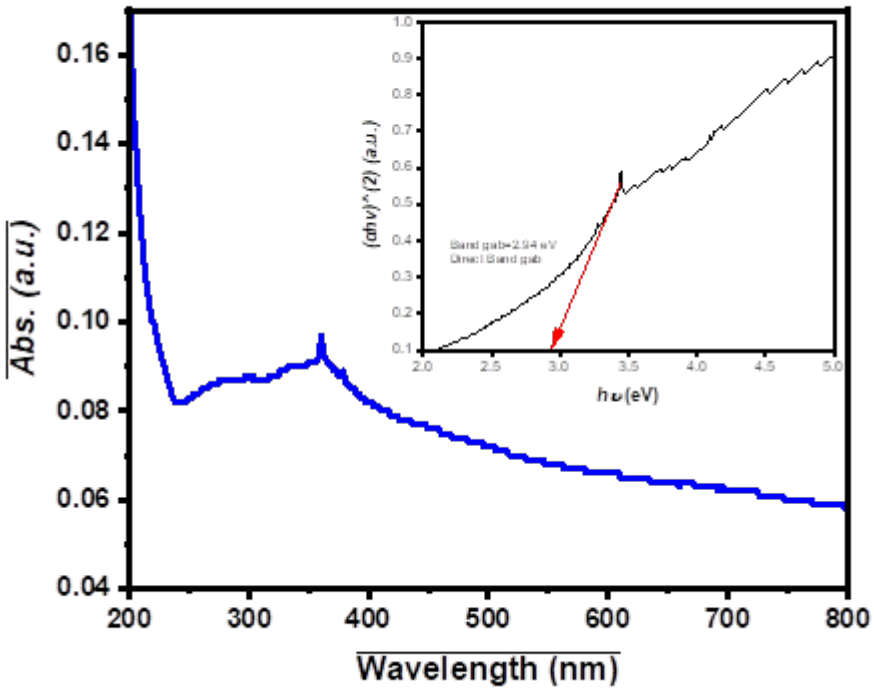

Fig. 4. UV-Vis absorption spectrum of the ZnS-ZnO nanoparticles grown at pH (12) for (1 h) with (20%) HMT, along with the corresponding Tauc plot for estimating the direct effective optical band gap.

Upon increasing the ZnS-ZnO content to 1wt% in sample P2, a weak shoulder appears in the 2θ range of approximately 26.73-28.04°. These features can be indirectly assigned to the (100) plane of hexagonal ZnS and the (111) plane of cubic ZnS, respectively. Nevertheless, the absence of sharp and well-defined ZnS and ZnO diffraction peaks indicates that the nanoparticles remain highly dispersed and retain a very small crystallite size, even at higher loading levels. Overall, the XRD results demonstrate that increasing the ZnS-ZnO concentration in the range of (6wt%to 1wt%) induces limited nucleation without promoting significant crystal growth, thereby preserving the semi-amorphous nature of the ZnS-ZnO/PVA nanocomposite films. This structural configuration is highly desirable for optical and optoelectronic applications, as it minimizes light scattering and suppresses defect-related non-radiative recombination losses, while maintaining the intrinsic transparency of the PVA matrix [31].

FESEM Analysis of ZnS-ZnO/PVA Nanocomposite Films

Fig. 6A-c shows FESEM images of the surface of the pure PVA film (Po) and ZnS-ZnO/PVA nanocomposite films with ZnS-ZnO loadings of 6wt% sample P1 and 1wt%sample P2. FESEM images of sample Po in Fig. 6A-a confirmed the formation of a smooth and homogeneous surface without visible crystalline regions or large aggregates. This appearance indicates that the polymer chains were largely reorganized into an amorphous arrangement during solvent evaporation. As the water gradually diffused out of the matrix, the hydrophilic PVA chains were able to rearrange themselves through internal hydrogen bonding, resulting in a continuous and uniform film rather than separated structures. These results were consistent with a previous study [32].

The findings of FESEM images in Fig. 6B-b of sample P1 displays a fairly homogeneous distribution at the nanoscale of the ZnS-ZnO compound (0.6 wt%) within the PVA matrix, indicating effective stabilization of the nanoparticles through hydrogen bonding interactions between the polymer chains and the ZnS-ZnO surfaces. This homogeneous distribution suggests that at low filler content, the PVA

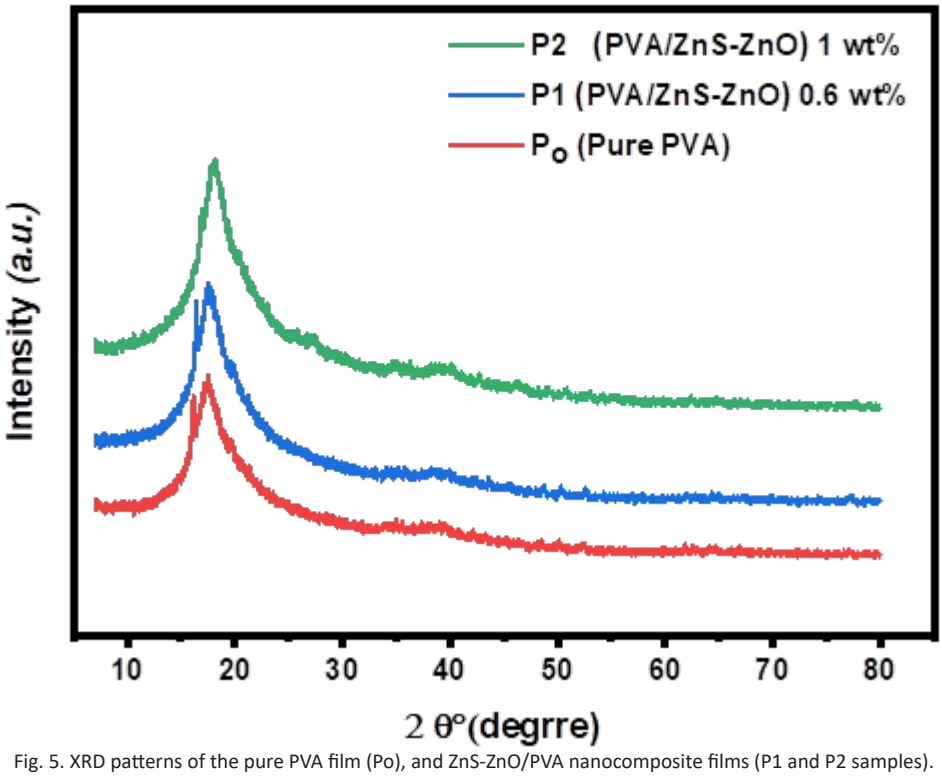

Fig. 5. XRD patterns of the pure PVA film (Po), and ZnS-ZnO/PVA nanocomposite films (P1 and P2 samples).

matrix effectively restrains the agglomeration of nanoparticles and enhances structural continuity. In contrast, increasing the ZnS-ZnO loading to 1wt% in sample P2 leads to a noticeable morphological evolution, as shown in FESEM images in Fig.6 C-c. Where bright, nearly spherical surface features become evident, which are attributed to the initial formation of ZnS-ZnO clusters resulting from partial nanoparticle aggregation. This behavior indicates that, at higher filler concentrations, the stabilizing effect of hydrogen bonding within the PVA matrix becomes insufficient to fully prevent interparticle interactions and cluster formation. Despite the onset of aggregation in sample P2, the

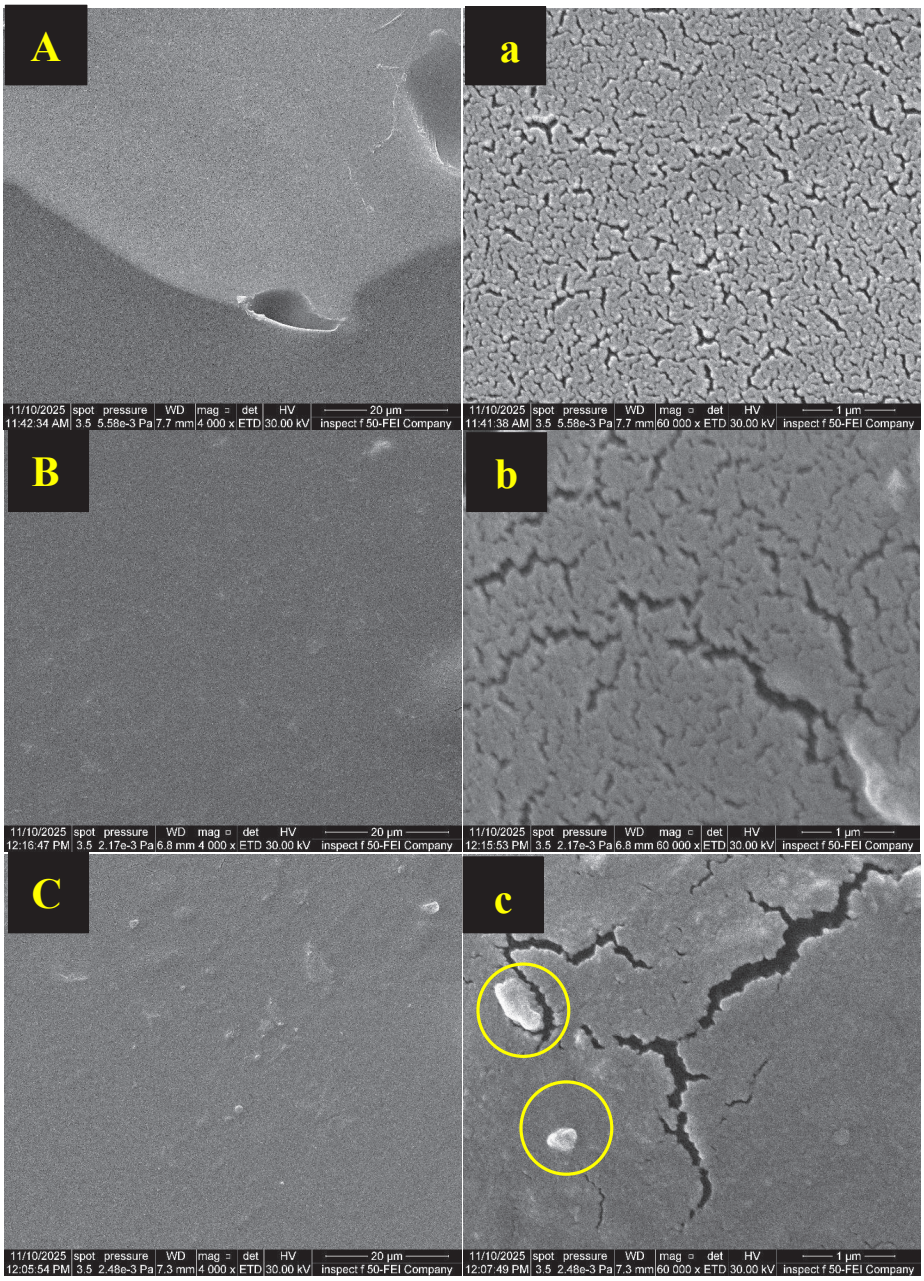

Fig. 6 (A-c). FESEM images of hydrothermally synthesized samples: (A-a) pure PVA Film (Po), (B-b) ZnS-ZnO/PVA nanocomposite Film with 0.6 wt% loading (P1), and (C- c) ZnS- ZnO/PVA nanocomposite film with 1 wt% loading (P2).

nanocomposite films remain structurally intact. Furthermore, the appearance of fine surface cracks is observed, which can be attributed to shrinkage stresses generated during solvent evaporation and film drying. Such morphological features are commonly reported in solution-cast PVA-based nanocomposite films at elevated filler loadings.

Overall, the observed transition from a smooth and homogeneous surface (P1) to a partially aggregated morphology (P2) is characteristic of ZnS-ZnO/PVA nanocomposites and is expected to influence surface roughness and optical response, particularly light scattering and defect-assisted recombination processes [33].

Optical properties of ZnS-ZnO/PVA Films

Fig. 7 illustrates the UV-Vis absorption spectra of as-synthesised ZnS-ZnO/PVA films by the hydrothermal method at precursor pH = 12, t = 1 h, HMT (20%) and T= 100 °C, which reveals a clear and systematic evolution in optical behaviour as the ZnS-ZnO loading increases from 6wt%to 1wt%. From the obtained results, a pronounced and progressive enhancement in absorption intensity is observed in the deep ultraviolet region in the range of (260 nm to 360 nm), which can be attributed to the increasing concentration of optically active ZnS-ZnO nanoparticles embedded within the PVA matrix. As well as the strengthening of characteristic band-to-band electronic transitions of ZnO and ZnS. This trend is consistent with recent studies reporting that the incorporation of ZnS-ZnO into PVA significantly enhances UV absorption and alters the optical band structure compared with pristine polymer films [34].

At a lower ZnS-ZnO concentration (P1, 6wt%), a slight elevation of the spectral baseline in the visible region is detected, indicating an increase in the number of ZnS-ZnO/PVA interfacial regions and

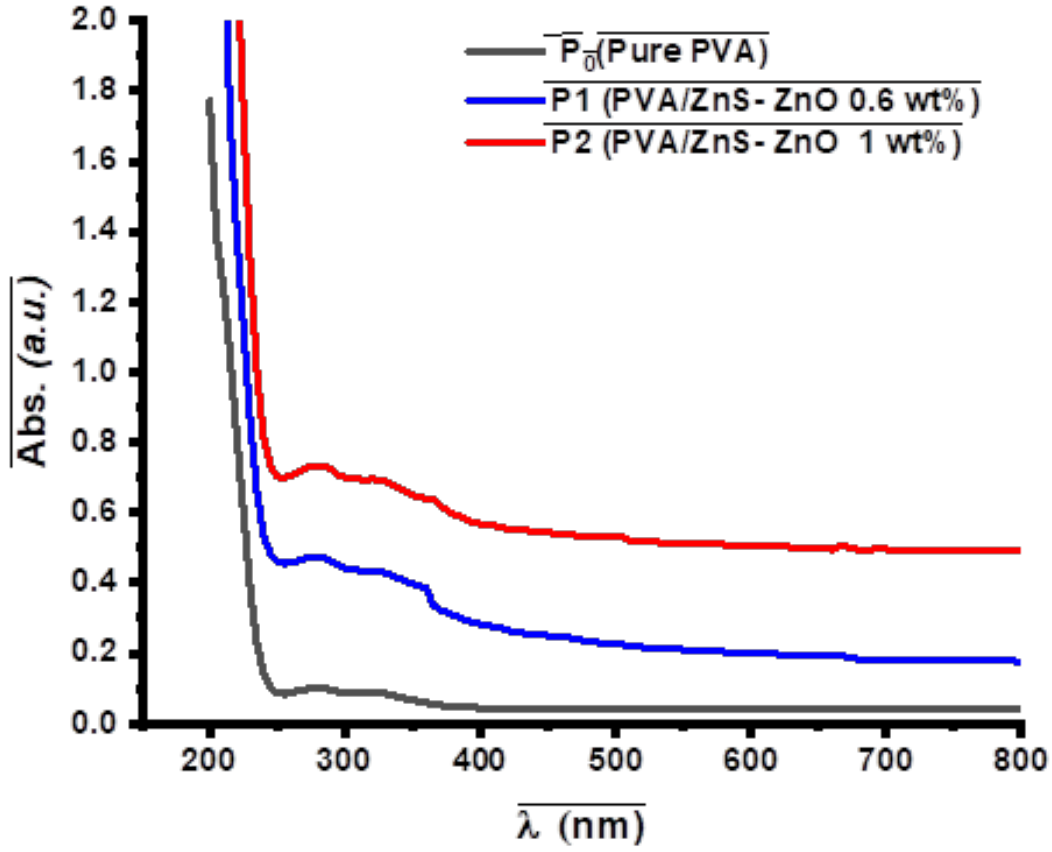

Fig. 7. UV-Vis absorption spectra of pure PVA and ZnS-ZnO/PVA films with different ZnS-ZnO nanoparticles loading ratios (0.6-1 wt%).

the initial emergence of defect-related electronic states, without causing a significant deterioration in optical transparency. This modest background absorption can be correlated with the higher nanoparticle density and the associated increase in light scattering within the composite matrix. In contrast, at the higher ZnS-ZnO concentration of 1wt%of sample P2, a more pronounced absorption tail extends into the visible region, accompanied by a marked increase in overall absorption intensity. This behavior suggests that the system approaches a near-saturation regime, in which nanoparticle agglomeration and the formation of sub-bandgap defect states become increasingly influential. In this regime, the optical response is governed by a delicate interplay between quantum confinement

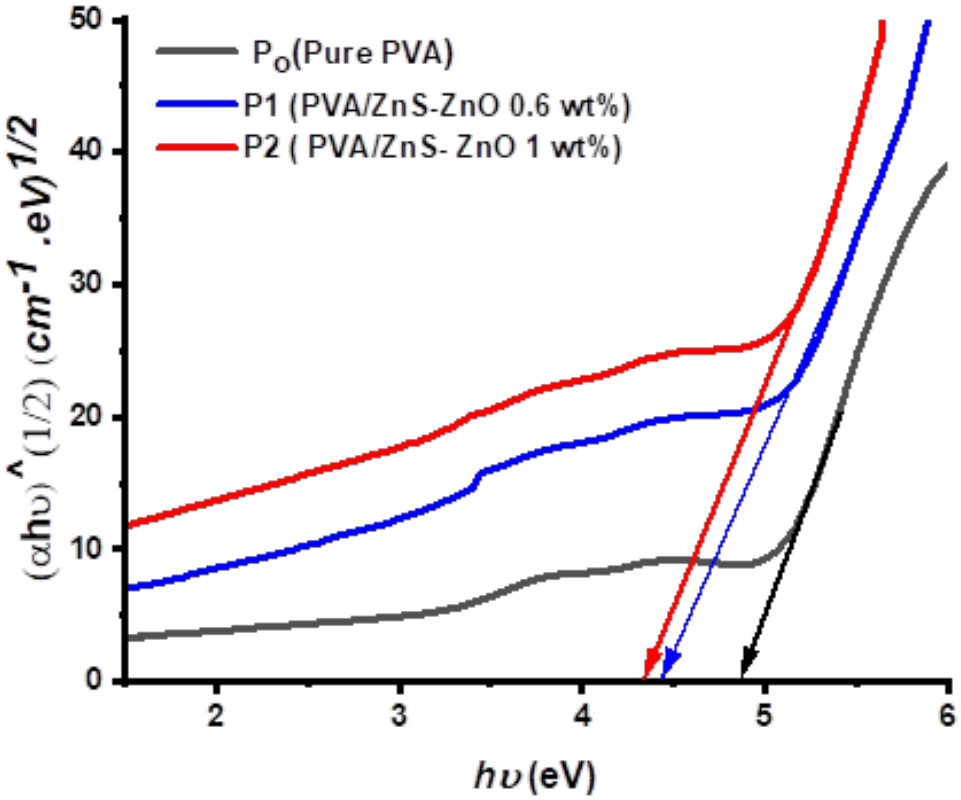

Fig. 8. Tauc plots for the allowed indirect optical band gap of Po, P1, and P2 ZnS-ZnO/PVA films.

Table 2. Optical band gap (Eg) values of Pure PVA Film, and ZnS-ZnO/PVA Films.

Samples	Eg(eV)	PVA/ZnS-ZnO (wt %)
ZnS-ZnO	2.94	-
PVA(Pure)	4.9	-
ZnS-ZnO/PVA	4.48	0.6 w t %
ZnS-ZnO/PVA	4.36	1 w t %

effects, surface defect states, and nanoparticle clustering.

Overall, the ZnS-ZnO/PVA nanocomposite clearly demonstrates a transition from a lightly ratio, optically transparent system to a near-saturation regime dominated by strong ultraviolet absorption. The highest UV-shielding efficiency is achieved at a ZnS-ZnO loading of 1wt%, albeit at the expense of a moderate reduction in visible transparency. This behaviour is in excellent agreement with the general trends reported for ZnS-ZnO/PVA nanocomposites, where increasing ZnS-ZnO content leads to a gradual broadening of the UV absorption band and a noticeable shift of the absorption edge [33].

Furthermore, the optical energies bandgap (Eg) of the Po, P1, and P2 samples, consisting of pure PVA and ZnS-ZnO/PVA films were estimated using Tauc plots as a function of photon energy, as illustrated in Fig. 8. The extracted bandgap values for pristine PVA, pure ZnS-ZnO nanoparticles, and ZnS-ZnO/PVA nanocomposite films with different ZnS-ZnO loadings (0.6 wt% to 1 wt%) are summarized in Table 2.

Pure PVA (sample Po) film exhibits a wide optical bandgap of approximately 4.9 eV, which is consistent with its insulating polymeric nature. Upon incorporation of ZnS-ZnO NPs, a gradual reduction in the Eg value from (4.48 eV to 4.36 eV) of the nanocomposite films is observed with increasing ZnS-ZnO content, as confirmed by Fig. 8. This behaviour can be attributed to the enhanced contribution of interfacial states, defect-related absorption, and localized energy levels introduced by the ZnS-ZnO nanoparticles within the PVA matrix, which effectively narrow the optical bandgap of as-grown film[35, 36]. The higher decrease in the Eg (4.36 eV) is observed at the highest ZnS-ZnO NPs loading (1wt%). This gradual bandgap reduction reflects improved nanoparticle dispersion and a more balanced interfacial interaction under alkaline synthesis conditions, as further supported by the XRD and FESEM analyses results in this study.

CONCLUSION

In this study, a ZnS-ZnO binary nanocomposite was successfully synthesized using the simple hydrothermal method and effectively incorporated into a polyvinyl alcohol (PVA) polymer matrix to produce homogeneous nanocomposite films with good mechanical stability. X-ray diffraction (XRD) analysis confirmed that the ZnS-ZnO system exhibits a stable multiphase crystalline structure. The crystallite size of the ZnS phase was found to be smaller than that of ZnO, indicating controlled crystal growth and a reduction in structural defects within the composite. FESEM findings revealed a uniform dispersion of ZnS-ZnO nanoparticles at a lower loading concentration (0.6 wt%), while partial agglomeration was observed at higher content (1 wt%). This behaviour highlights the important role of the PVA matrix in stabilizing the nanoparticles and limiting their aggregation. UV-Vis spectroscopic measurements demonstrated a significant enhancement in ultraviolet absorption while maintaining high transparency in the visible region. Additionally, a gradual decrease in the effective optical band gap from 4.48 eV to 4.36 eV was observed with increasing ZnS-ZnO NPs content. This reduction is attributed to the formation of new energy states and improved electronic interactions between the nanoparticles and the polymer matrix. Overall, the results indicate that incorporating ZnS-ZnO nanocomposites into PVA films enables the development of flexible nanomaterials with tuneable optical properties and strong UV-shielding capability. These characteristics make the fabricated ZnS-ZnO/PVA film promising candidates for applications in optoelectronic devices, UV-protective coatings, and optical sensors.

ACKNOWLEDGEMENTS

The researchers would like to express their gratitude to the Department of Physics, College of Science, Mustansiriyah University, for their support in achieving this work.

CONFLICT OF INTEREST

The authors declare that there is no conflict of interests regarding the publication of this manuscript.

REFERENCES

1. Liu L, Wang L, Sun D, Sun X, Liu L, Zhao W, et al. ZnO-ZnS Heterostructure as a Potent Photocatalyst in the Preparation of Some Substituted Chromenes and Remarkable Antigastrointestinal Cancer Activity. ACS Omega. 2023;8(46):44276-44286.
2. Sunaina, Devi S, Nishanthi ST, Mehta SK, Ganguli AK, Jha M. Surface photosensitization of ZnO by ZnS to enhance the photodegradation efficiency for organic pollutants. SN Applied Sciences. 2021;3(7).
3. Jin X, Chen J, Chen F, Duan H, Wang Z, Li J. Solid-State Synthesis of ZnO/ZnS Photocatalyst with Efficient Organic Pollutant

Degradation Performance. Catalysts. 2022;12(9):981.
4. Jiang Y, Meng XM, Liu J, Hong ZR, Lee CS, Lee ST. ZnS Nanowires with Wurtzite Polytype Modulated Structure. Adv Mater. 2003;15(14):1195-1198.
5. Zhu YC, Bando Y, Xue DF, Golberg D. Oriented Assemblies of ZnS One-Dimensional Nanostructures. Adv Mater. 2004;16(9-10):831-834.
6. Zhang H, Zhang S, Zuo M, Li G, Hou J. Synthesis of ZnS Nanowires and Assemblies by Carbothermal Chemical Vapor Deposition and Their Photoluminescence. Eur J Inorg Chem. 2004;2005(1):47-50.
7. Xu X-J, Fei G-T, Yu W-H, Wang X-W, Chen L, Zhang L-D. Preparation and formation mechanism of ZnS semiconductor nanowires made by the electrochemical deposition method. Nanotechnology. 2005;17(2):426-429.
8. Bengas R, Lahmar H, Redha KM, Mentar L, Azizi A, Schmerber G, et al. Electrochemical synthesis of n-type ZnS layers on p-Cu_2O/n-ZnO heterojunctions with different deposition temperatures. RSC Advances. 2019;9(50):29056-29069.
9. Ali S, Saleem S, Salman M, Khan M. Synthesis, structural and optical properties of ZnS–ZnO nanocomposites. Materials Chemistry and Physics. 2020;248:122900.
10. Piña-Pérez Y, Aguilar-Martínez O, Acevedo-Peña P, Santolalla-Vargas CE, Oros-Ruíz S, Galindo-Hernández F, et al. Novel ZnS-ZnO composite synthesized by the solvothermal method through the partial sulfidation of ZnO for H_2 production without sacrificial agent. Applied Catalysis B: Environmental. 2018;230:125-134.
11. Rabenau A. The Role of Hydrothermal Synthesis in Preparative Chemistry. Angewandte Chemie International Edition in English. 1985;24(12):1026-1040.
12. Walton RI. Subcritical solvothermal synthesis of condensed inorganic materials. Chem Soc Rev. 2002;31(4):230-238.
13. Zhao J, Zhao L, Wang X. Preparation and characterization of ZnO/ZnS hybrid photocatalysts via microwave-hydrothermal method. Frontiers of Environmental Science and Engineering in China. 2008;2(4):415-420.
14. Young RJ, Lovell PA. Introduction to Polymers. CRC Press; 2011. http://dx.doi.org/10.1201/9781439894156
15. Jones JI. Polyvinyl alcohol. Properties and applications. Edited by C. A. Finch. John Wiley, Chichester. 1973. Pp. xviii + 622. Price: £14.00. British Polymer Journal. 1973;5(6):493-494.
16. Alshammari AH. Structural, Optical, and Thermal Properties of PVA/SrTiO3/CNT Polymer Nanocomposites. Polymers. 2024;16(10):1392.
17. Biswas S, Kar S. Fabrication of ZnS nanoparticles and nanorods with cubic and hexagonal crystal structures: a simple solvothermal approach. Nanotechnology. 2008;19(4):045710.
18. Al-Dhahir TA, Entisar EA-A, Tagreed MA-S, Latif I. Zno nanoparticles: Synthesis and crystal structure study. Journal of Wasit for Science and Medicine. 2023;7(3):87-95.
19. Bayram Ü, Özer Ç, Yilmaz E. Comparison of Photocatalytic and Adsorption Properties of ZnS@ZnO, CdS@ZnO, and PbS@ZnO Nanocomposites to Select the Best Material for the Bifunctional Removal of Methylene Blue. ACS Omega. 2025;10(10):9986-10003.
20. Anaya-Zavaleta JC, Ledezma-Pérez AS, Gallardo-Vega C, Rodríguez-Hernández J, Alvarado-Canché CN, García-Casillas PE, et al. ZnO Nanoparticles by Hydrothermal Method: Synthesis and Characterization. Technologies. 2025;13(1):18.
21. Abbas SAH, Hassan ES, Abdulmunem OM. Growth of Different Zinc Oxide Nanostructures under Hydrothermal pH Values. Baghdad Science Journal. 2024;21(7):2433.
22. Saranya A, Devasena T, Sivaram H, Jayavel R. Role of hexamine in ZnO morphologies at different growth temperature with potential application in dye sensitized solar cell. Mater Sci Semicond Process. 2019;92:108-115.
23. Abbas KN, Bidin N, Sabry RS, Al-Asedy HJ, Al-Azawi MA, Islam S. Structures and emission features of high-density ZnO micro/nanostructure grown by an easy hydrothermal method. Materials Chemistry and Physics. 2016;182:298-307.
24. Marakhovskiy MA, Talanov MV. Technological methods for reducing the sintering temperature of ceramics based on the BZN cubic pyrochlore system. Izvestiâ Akademii nauk SSSR Seriâ fizičeskaâ. 2024;88(5):800-804.
25. Mahdizadeh R, Sangpour P, Emrooz HBM. Surface texture dependency of photocatalytic behavior of facile synthesized mesoporous ZnS-ZnO heterostructure under LED illumination. Sci Rep. 2025;15(1).
26. Olumurewa KO, Eleruja MA. Tuning the properties of ZnxS1-x nanoparticles by controlling reaction conditions. Results in Chemistry. 2022;4:100476.
27. Tazim TQ, Kawsar M, Sahadat Hossain M, Bahadur NM, Ahmed S. Hydrothermal synthesis of nano-metal oxides for structural modification: A review. Next Nanotechnology. 2025;7:100167.
28. Al-Farsi L, Souier TM, Al-Hinai M, Myint MTZ, Kyaw HH, Widatallah HM, et al. pH Controlled Nanostructure and Optical Properties of ZnO and Al-Doped ZnO Nanorod Arrays Grown by Microwave-Assisted Hydrothermal Method. Nanomaterials. 2022;12(21):3735.
29. Yang TL, Lin PY, Fu YS, Luo CY, Hsu KC. Synthesis and photocatalytic performance of ZnS nanoparticles via electrospinning assisted hydrothermal technique. Chalcogenide Letters. 2025;22(7):625-636.
30. Dengo N, Vittadini A, Natile MM, Gross S. In-Depth Study of ZnS Nanoparticle Surface Properties with a Combined Experimental and Theoretical Approach. The Journal of Physical Chemistry C. 2020;124(14):7777-7789.
31. Kharazmi A, Faraji N, Mat Hussin R, Saion E, Yunus WMM, Behzad K. Structural, optical, opto-thermal and thermal properties of ZnS–PVA nanofluids synthesized through a radiolytic approach. Beilstein Journal of Nanotechnology. 2015;6:529-536.
32. Hamaamin OK, Ghareeb HO, Mohammed SJ. Eco-friendly enhancement of optical and structural properties in polyvinyl alcohol films via eggplant peel dye doping. Sci Rep. 2025;15(1).
33. Guruswamy B, Ravindrachary V, Shruthi C, Sagar RN, Hegde S. Optical, thermal and morphological study of ZnS doped PVA polymer nano composites. AIP Conference Proceedings: Author(s); 2018. p. 030211.
34. Gupta N, Chandel ALS, Mehta M, Tiwari A. Polyvinyl alcohol stabilized ZnS nanoaggregates using organosulfur source for photocatalytic disintegration of methyl orange dye. Results in Chemistry. 2024;7:101242.
35. Saadeldin MM, Samir A. Zinc tin oxide/polyvinyl alcohol nanocomposites enable sensitive pH-dependent arsenic detection by quartz crystal microbalance. Sci Rep. 2025;15(1).
36. Satheesh Goud J, Srinivas C, Narsimlu N. Preparation and spectroscopic studies of ZnO incorporated PVA nanocomposite films. Materials Today: Proceedings. 2022;67:872-878.